3D Targets for Evaluating Fingerprint Readers

Sunpreet S. Arora, *Student Member, IEEE,* Kai Cao, Anil K. Jain, *Life Fellow, IEEE,*
and Nicholas G. Paulter Jr., *Fellow, IEEE*

Abstract—Standard calibration targets are typically used for calibrating the imaging pathway of fingerprint readers. However, there is no standard method for evaluating fingerprint readers in the operational setting where variations in finger placement by the user are encountered. The goal of this research is to design 3D targets for repeatable operational evaluation of fingerprint readers. 2D calibration patterns with known characteristics (e.g. sinusoidal gratings of pre-specified orientation and frequency, synthetic fingerprints with known singular points and minutiae) are projected onto a generic 3D finger surface to create electronic 3D targets. A state-of-the-art 3D printer (Stratasys Objet350 Connex) is used to fabricate the 3D targets with material similar in hardness and elasticity to the human finger skin. Our experimental results show that the (i) fabricated 3D targets can be imaged using three different (500/1000 ppi) commercial optical fingerprint readers, (ii) salient features in the 2D calibration patterns are preserved during the synthesis and fabrication of 3D targets, and (iii) intra-class variability between multiple impressions of the 3D targets captured using the optical fingerprint readers does not degrade the recognition accuracy. We also conduct experiments to demonstrate that the fabricated 3D targets can be used for operational evaluation of fingerprint readers.

Keywords—3D targets, fingerprint reader evaluation, 2D calibration patterns, 3D printing, 2D pattern to 3D surface projection.

1 Introduction

Calibration of imaging systems typically involves the use of specially designed objects with known properties, called *calibration targets*. In the biomedical domain, for instance, such objects (called *phantoms*) are used for calibrating and testing optical measurement profiles of sensing instrumentation [2], [3]. Similarly, calibration targets (Fig. 1) are also used for calibrating fingerprint readers.

There are two separate standards currently in use by the Federal Bureau of Investigation (FBI) for the certification of fingerprint readers, (i) the *PIV-071006*, which caters to single finger readers designed for applications involving person verification (one-to-one comparison), and (ii) the *Appendix F*, which applies to fingerprint readers designed for use in large scale applications involving person identification (one-to-many comparisons). The *Appendix F* standard has more stringent image quality requirements compared to the *PIV-071006* standard [5]. To get their readers certified, fingerprint vendors need to demonstrate that the images captured using their readers meet the image quality specifications laid out in the relevant standard [4] [6]. A typical procedure is (i) to use 2D/3D calibration targets to ascertain if the images of the targets captured using the reader meet the standard specifications, (ii) modify the reader configuration, if needed, to ensure it captures images of sufficient quality to meet the specifications, and (iii) when satisfied with the reader configuration, submit test images to the testing agency for review[1] [5]. Furthermore, the testing agency reviews the test data to verify that the submitted images meet the image quality specifications. If the test data is found to meet the desired specifications, the testing agency certifies the fingerprint reader as being compliant with the specific standard.

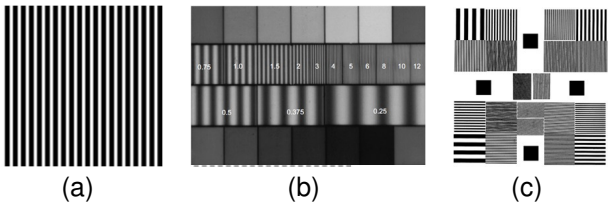

Fig. 1. 2D images of targets used for calibrating fingerprint readers, (a) ronchi (vertical bar) target for calibrating the geometric accuracy, (b) sine wave target for measuring the resolution, and (c) multiple bar target for estimating the spatial frequency response of a fingerprint reader (images taken from [4]).

The testing and certification of biometric devices for use by Unique Identification Authority of India (UIDAI) in the Aadhaar project in India is performed by the Standardization Testing and Quality Certification (STQC)

- *S. S. Arora and A. K. Jain are with the Department of Computer Science and Engineering, Michigan State University, East Lansing, MI, 48824. E-mail: {arorasun, jain}@cse.msu.edu*
- *K. Cao is with the Department of Computer Science and Engineering, Michigan State University, East Lansing, MI, 48824, and with the School of Life Sciences and Technology, Xidian University, Xi'an, Shaanxi 710126, China. Email: kaicao@cse.msu.edu*
- *N. G. Paulter Jr. is with the National Institute of Standards and Technology, 100 Bureau Dr., Gaithersburg, MD, 20899. E-mail: paulter@nist.gov*
- *An earlier version of this paper appeared in the proceedings of the 22nd International Conference on Pattern Recognition (ICPR), 2014 [1].*

1. Review of the submitted test data is conducted by the Technology Evaluation Standards Test Unit, Biometric Center of Excellence (BCOE) led by the Criminal Justice Information (CJI) Services Division [7].

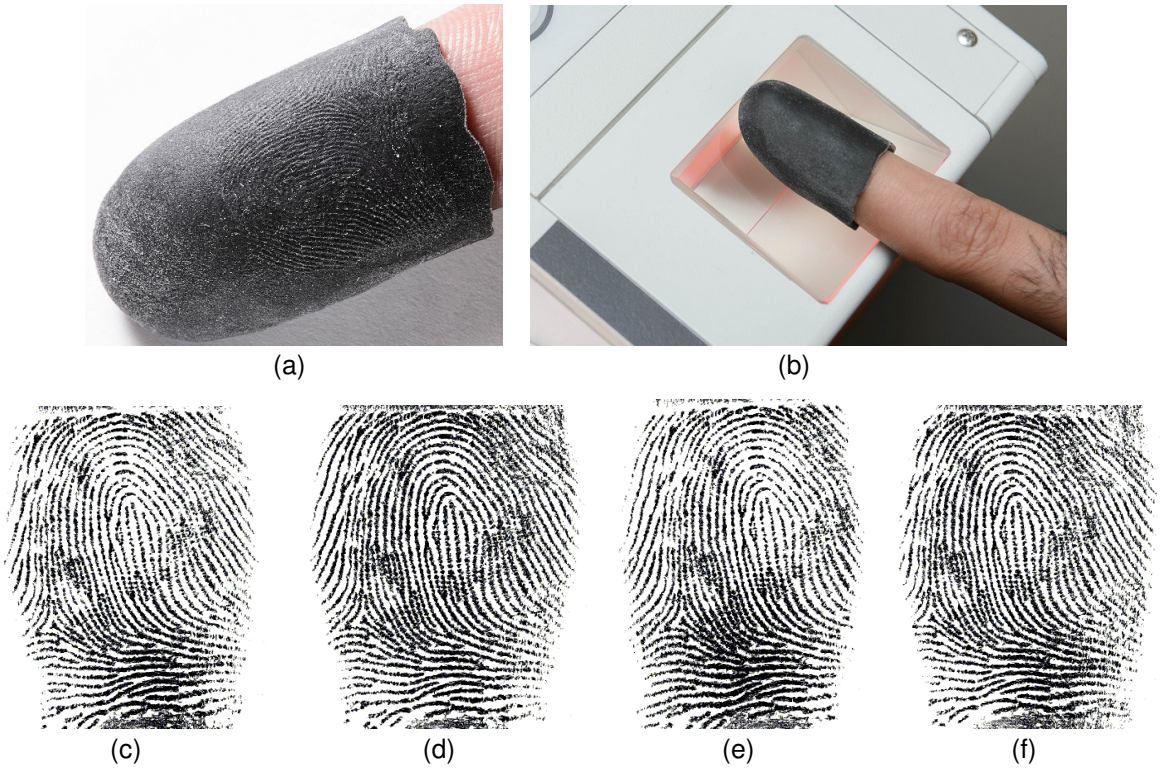

Fig. 2. Evaluating an optical fingerprint reader using the 3D targets designed and fabricated by the authors. (a) The 3D target is worn on a finger, (b) the finger is repeatedly placed on the fingerprint reader platen, and (c)-(f) multiple 2D impressions (four shown here) of the 3D target are captured which are utilized for evaluation of the reader.

Directorate, Government of India [8]. UIDAI is one of the largest consumers of biometric readers in the world, with currently, there being 36,000 enrolment stations deploying 11 different certified biometric readers in Aadhaar [9]. Image acquisition requirements equivalent to Appendix F are mandated for fingerprint readers used for enrolment in Aadhaar [10]. For getting their readers certified, fingerprint vendors submit a certification agreement to the certification agency, the STQC Directorate. The certification agency evaluates the evidence of conformity of the submitted agreement to the certification procedure guidelines. Thereafter, the STQC directorate tests the fingerprint reader in the lab to determine if it meets the standard specifications. Provided that the testing procedure results are satisfactory, the fingerprint reader is certified by the agency for use in Aadhaar [11].

Standard calibration targets can be used for calibrating the imaging pathway of a fingerprint reader. For example, the targets in [15] can be utilized for testing the frustrated total internal reflection (FTIR) pathway of an optical fingerprint reader. However, they cannot be used to evaluate a fingerprint reader for variations encountered operationally during the fingerprint capture process, e.g., application of different finger pressure on the reader platen, and placement of the finger in different ways by the user. This is because these targets are not specifically fabricated using materials similar in properties to the human finger skin. Hence, it is not possible to mimic the typical fingerprint acquisition scenario using these targets, which involves the placement of finger with certain pressure on the fingerprint reader.

For operational evaluation of a fingerprint reader, one possibility, therefore, is to conduct pilot studies in the field using the fingerprint reader. This, however, is a tedious process both in terms of time and resource commitment, and is limited by the amount and nature of data collected. Besides, such a procedure cannot be used for repeatable operational evaluation of the fingerprint reader because, in practice, the same set of subjects is typically not available for repeated testing. The goal of this research, therefore, is to fabricate standard 3D targets which can be used for repeatable operational evaluation of fingerprint readers. We fabricate 3D targets with material similar in hardness and elasticity to the human finger skin specifically such that they can be worn on a finger and placed on the fingerprint reader platen in a natural manner (see Fig. 2).

The utility of the fabricated 3D targets extends beyond evaluation of fingerprint readers. 3D targets created by projecting 2D synthetic fingerprint images with known fingerprint features (e.g. type, minutiae and singular point locations) onto the 3D finger surface can be used

TABLE 1
Comparison of existing fingerprint system evaluation methods with the proposed 3D target creation method

Method	Artifacts	Fingerprint Features	Evaluation Use Cases
SFinGe [12]	2D synthetic fingerprints (electronic)	Known fingerprint ridge flow and ridge density features; uncontrolled minutiae placement	Fingerprint feature extractors and matchers
IBG DHS SBIR [13]	2D synthetic fingerprints (electronic)	Known fingerprint ridge flow, ridge density features; partially controlled minutiae features	Fingerprint feature extractors and matchers
Zhao et al. [14]	2D synthetic fingerprints (electronic)	Known fingerprint ridge flow, ridge density and minutiae features	Fingerprint feature extractors and matchers
Proposed	3D targets (electronic and physical)	Known fingerprint ridge flow, ridge density and minutiae features	End-to-end fingerprint systems, including fingerprint readers, feature extractors and matchers

to evaluate fingerprint feature extraction and matching algorithms. Such targets can, therefore, be used for end-to-end evaluation of a fingerprint recognition system from placing the finger on the reader and capturing the 2D impression to extracting features and matching the captured image to the gallery templates. This is better than the existing methods which only use 2D synthetic fingerprint images for evaluation purposes (see Table 1).

A physical 3D target is created by projecting an electronic 2D calibration pattern onto a generic electronic 3D model of the finger surface[2]. The electronic 3D finger surface is first aligned such that the finger length is along the y-axis, width along the x-axis and depth along the z-axis. The electronic 3D finger surface is then preprocessed to ensure sufficient fidelity for approximately determining the correspondences between the electronic 2D calibration pattern and the electronic 3D finger surface. The electronic 2D calibration pattern is then mapped onto the front portion of the electronic 3D finger surface and correspondences between each vertex on the frontal electronic 3D surface and the pixel locations in the electronic 2D calibration pattern are established. The electronic 2D calibration pattern is engraved onto the frontal electronic 3D finger surface by displacing each vertex along the surface normal according to the texture values at the mapped pixel locations. Finally, the electronic 3D finger surface is post-processed to create an electronic model of a wearable 3D target ready for 3D printing.

The physical 3D targets are fabricated using a state-of-the-art 3D printer (Stratasys Objet350 Connex[3]) with material similar in hardness and elasticity to the human finger skin. The targets are imaged using three different (500/1000 ppi) commercial optical fingerprint readers. Our experimental results show that the captured images of the physical 3D targets can be successfully matched to the electronic 2D synthetic fingerprint patterns used to generate the 3D targets using a commercial fingerprint SDK [17]. This demonstrates that the salient features present in the electronic 2D calibration pattern are essentially preserved when mapping it to the physical 3D surface of the fingerprint target. Experiments are also conducted to demonstrate that the intra-class variability between the different images of the 3D targets captured using the three optical readers is minimal. We also conduct experiments for operational evaluation of the three aforementioned optical fingerprint readers using the fabricated 3D targets.

2. The 3D finger surface could either be the shape of the finger sensed using a 3D fingerprint scanner or a synthetically generated surface describing the shape of the finger. In our case, the finger surface was scanned using the Artec Eva 3D scanner [16].

3. The naming of companies and products does not imply endorsement or recommendation of those companies or products by the authors or the organizations they represent.

2 Synthesizing 3D Targets

A 3D target A is synthesized from a 2D calibration pattern I with pre-specified features, and a generic 3D finger surface S. Let the texture feature value in the 2D calibration pattern I at spatial coordinates (u, v) be denoted by $I(u, v)$. Also, assume that the 3D finger surface S is a triangular mesh having a set of vertices V and triangles T. Each vertex, v, in V has (x, y, z) coordinates corresponding to its spatial location in S, and a triangle in T connects a unique set of three vertices. Synthesizing the 3D target A using I and S then consists of the following steps (Fig. 3) (details of the processes summarized below are given in Sections 2.1-2.6):

1) **Preprocessing 3D finger surface**: Align S such that the finger length is along the y-axis in S. Sample vertices from the set V based on the curvature of S. This sampling process reduces the density of S, therefore, subdivide S (as explained in Section 2.1) to ensure sufficient fidelity during projection of the 2D calibration pattern I. Displace S outwards along the direction of the surface normals computed at each vertex to create an outer finger surface S_O. Separate the front S_{OF} and rear portion S_{OR} of S_O (see Fig. 4). The front portion S_{OF} of S_O will be used for projection. Retain the original surface S.
2) **Preprocessing 2D calibration pattern**: If the pattern I being projected is a 2D fingerprint image, extract the skeleton I_S of the image I. Increase the ridge width of the skeleton I_S using morphological operations, and smooth the image using a Gaussian filter before projecting it onto the

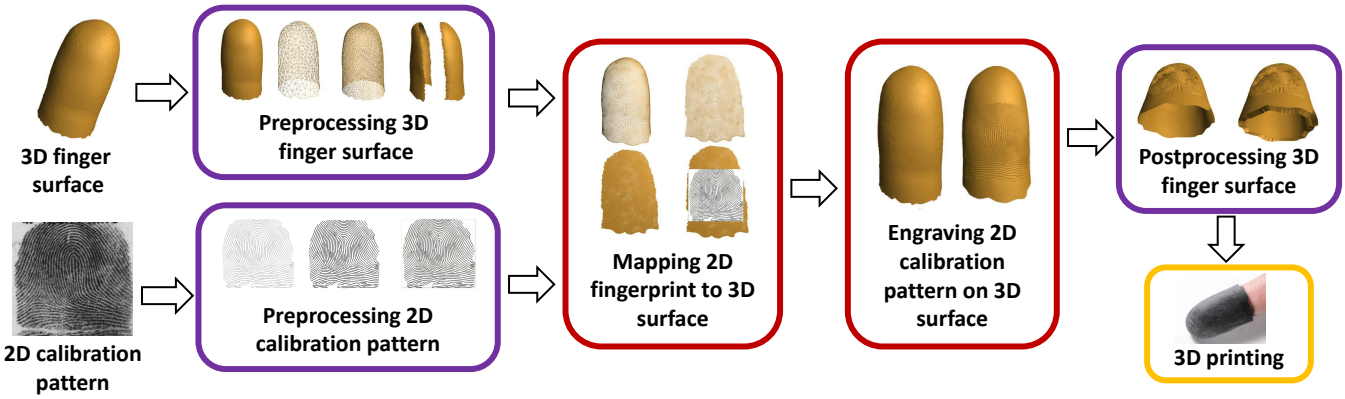

Fig. 3. Synthesizing a 3D target from a 2D calibration pattern and a 3D finger surface.

electronic frontal surface S_{OF}. This preprocessing step is necessary to ensure that ridges and valleys present in I are engraved smoothly onto S_{OF}. Note that this preprocessing step is not needed if any other 2D calibration pattern (e.g. sine grating) is being projected.

3) **Mapping 2D fingerprint to 3D surface**: Project the front portion S_{OF} of 3D finger surface S_O to 2D and correct for rotation and flip using corresponding control points between 3D surface S_{OF} and the 2D projection of S_{OF}, and translation with respect to reference coordinates computed from I. Make the front portion of the outer finger surface S_O dense depending on the resolution of I to ensure sufficient fidelity of mapping I. Determine the mapping between the (x, y, z) spatial locations of the vertices on the front portion of the outer 3D surface S_O and the (u, v) image domain of I.
4) **Engraving 2D calibration pattern on 3D surface**: To create ridges and valleys, displace the vertices on the front portion of S_O along the surface normals according to the texture values in I at the mapped (u, v) locations.
5) **Postprocessing 3D finger surface**: Combine the front and rear portions of the outer finger surface S_O. Make the original finger surface S as dense as the outer finger surface S_O and then stitch the two surfaces together to obtain a watertight solid target. This finishes the creation of the 3D target A as an electronic (virtual) target.
6) **3D Printing**: Specify the physical dimensions as well as the printing material according to the hardness and elasticity of the human finger skin before printing the 3D target A using a 3D printer (Stratasys Objet350 Connex).

A detailed description of each of these steps used in the 3D target creation process for a given 2D calibration pattern I and a 3D finger surface S is given below.

2.1 Preprocessing 3D finger surface

A sequence of preprocessing steps are executed on the 3D finger surface S before projecting the 2D calibration pattern I (see Fig. 4).

Alignment

The 3D finger surface S, arbitrarily oriented in the (x, y, z) coordinate frame, is first aligned such that the finger length is along the y-axis, width along the x-axis and height on the z-axis. For doing this, each vertex in the set V is translated such that the center of the surface S coincides with the origin of the (x, y, z) coordinate axes. Principal component analysis (PCA) [18] is used to determine the principle directions of the surface spread. The computed principal components are then used to align the surface S. Note that this step only alters the absolute (x, y, z) coordinate values of the vertices in V and retains the geometry of the surface S.

Remeshing

The 3D finger surface S is remeshed by sampling vertices from V using the method described in [19]. The first vertex v_1 is sampled randomly from V, and the geodesic distance map $U(v_1)$ from v_1 to every other vertex in V is computed by solving the eikonal equation using the fast marching method [20]:

$$||\Delta U(v_1)|| = P(v_1). \quad (1)$$

Here, Δ is the gradient operator, and $P = 1/F$, where F is the speed of front propagation used in the fast marching method.

Vertices are then sampled iteratively by adding the farthest vertex among the remaining vertices in iteration i from the vertices in the sampled vertex set V_{i-1} at iteration $i - 1$. Note that the geodesic distance map U_i, at iteration i, is updated using the following equation:

$$U_i = min(U_{i-1}, U(v_i)), \quad (2)$$

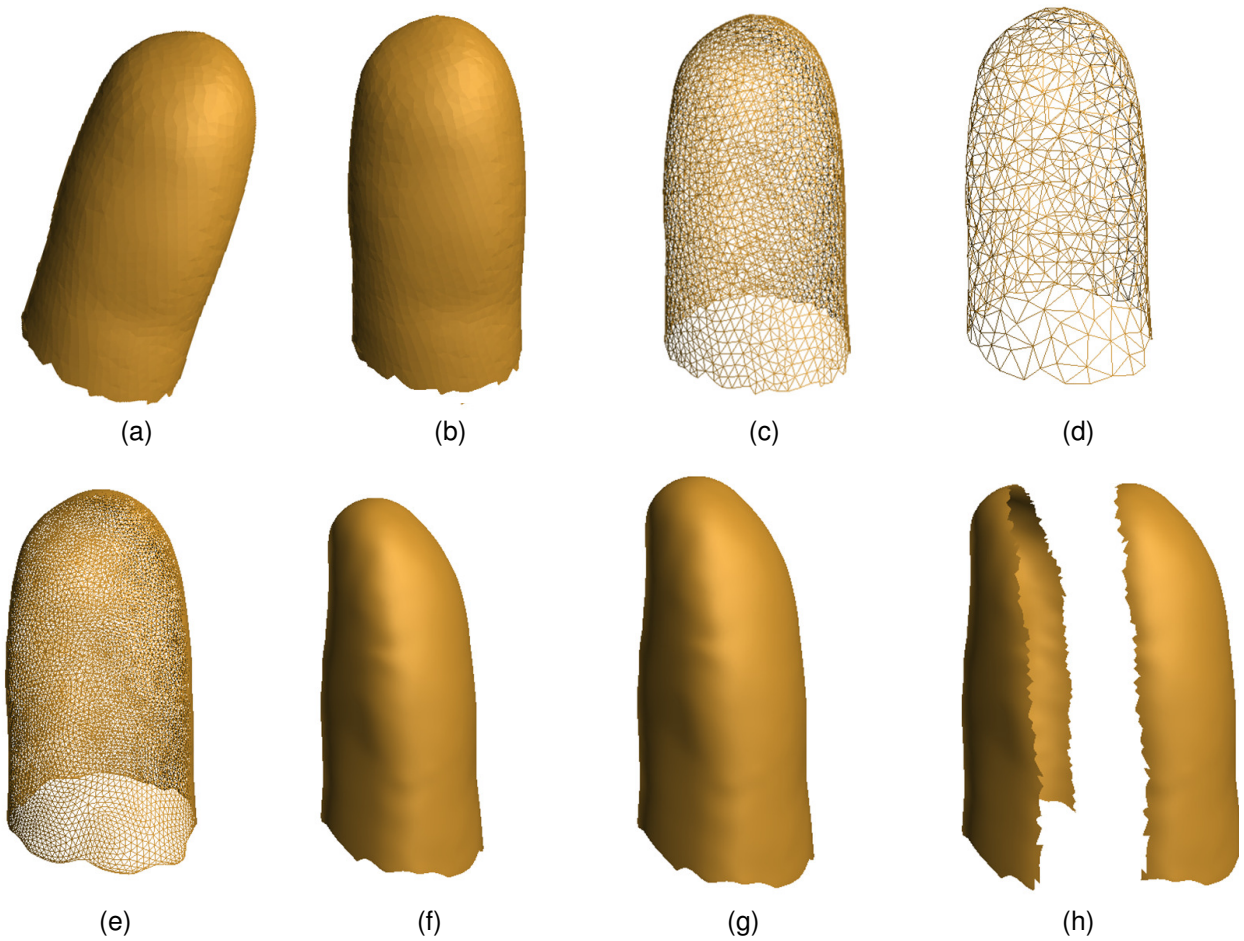

Fig. 4. Preprocessing 3D finger surface. (a) Original finger surface, (b) aligning the finger surface such that the finger length is along the y axis, (c) aligned finger surface (triangular mesh), (d) remeshing the finger surface (triangular mesh), (e) subdividing the surface (triangular mesh), (f) subdivided finger surface (profile view), (g) creating outer finger surface from (f), and (h) separating front and back portions of the outer finger surface.

where $U(v_i)$ is the geodesic distance map of the vertex sampled at iteration i, and U_{i-1} is the geodesic distance map computed at iteration $i-1$.

During this iterative procedure of sampling vertices, the speed of front propagation F is set to $1/(1+C)$, where C is the aggregate curvature at each vertex in V. This results in more vertices being sampled in the higher curvature regions of the 3D surface and vice versa. The aggregate curvature C is calculated using the two principal curvatures C_{min} and C_{max} as follows,

$$C = |C_{min}| + |C_{max}|. \tag{3}$$

Here, $|\ .|$ is the absolute value operator, C_{min} and C_{max} are computed from the 3D curvature tensor T calculated using the method in [21]. In particular, C_{min} and C_{max} correspond to the two highest eigenvalues of the curvature tensor T.

Finally, Delaunay triangulation is used for reconstructing the remeshed surface from the set of sampled vertices [22].

Subdivision

Although remeshing makes the surface S uniformly dense depending on its curvature, it reduces the surface density. To ensure sufficiently fidelity for projecting the 2D calibration pattern I onto the surface S, Loop's surface sub-division method [23] is used. Let the set of vertices and triangles obtained after remeshing be denoted by V_R and T_R, respectively. This method creates new vertices at each edge of every triangle in T_R using a weighted combination of neighborhood vertices, and creates new triangles by connecting the sampled vertices at edges adjacent to each other. The original vertices are then translated to maintain surface smoothness and continuity.

(a) (b) (c) (d)

Fig. 5. Preprocessing a 2D fingerprint pattern before projection onto 3D finger surface. (a) Original fingerprint image, (b) extracted skeleton of the fingerprint in (a), (c) skeleton in (b) after applying the morphological operation of dilation, and (d) dilated skeleton in (c) smoothed using a gaussian filter.

Creating outer surface

Let V_S and T_S be the set of vertices and triangles obtained after surface subdivision. Each vertex v in the set V_S is then displaced by a fixed factor d along the normal n computed at the vertex v:

$$\begin{bmatrix} v'_x \\ v'_y \\ v'_z \end{bmatrix} = \begin{bmatrix} v_x \\ v_y \\ v_z \end{bmatrix} + \begin{bmatrix} n_x \\ n_y \\ n_z \end{bmatrix} \times d \tag{4}$$

This is done to create an outer finger surface S_O where the 2D calibration pattern will be projected. The parameter d determines the thickness of the 3D target. Ideally, it is desirable to set d to be as small as possible. However, due to the limitation of the 3D printer resolution used for fabricating the targets, choosing a very small d results in the printed model being fragile. Therefore, d is empirically set to 1.5 mm in our experiments.

Separating front and rear portions

Front and rear portions of the outer finger surface S_O are then separated by computing the surface normals at each triangle in T_S, and then retaining the triangles and corresponding vertices where surface normals have the z-component greater than 0 in the front surface, and the rest in the rear surface. Note that the alignment of the finger surface done in step 1) facilitates this separation process. Let us denote the front portion of the outer surface S_O as S_{OF} having the set of vertices V_{OF} and triangles T_{OF}. Similarly, let the rear portion be denoted as S_{OR} with the set of vertices V_{OR} and triangles T_{OR}. Also, note that we retain the original finger surface S having the set of vertices V_S and triangles T_S.

2.2 Preprocessing 2D calibration pattern

If the pattern I being projected is a fingerprint image, the following preprocessing steps are executed on I:

1) The skeleton of I is extracted using a commercial fingerprint SDK [17]. The skeleton is a 1-pixel wide ridge pattern. Let the skeleton be denoted by I_S.
2) The ridge width on the skeleton I_S is increased to 3 pixels by performing the morphological operation of dilation using a 2 pixel radius disk structured element.
3) I_S is filtered using a 4×4 Gaussian filter with $\sigma = 2.5$. This is necessary to ensure that ridges and valleys present in the 2D fingerprint pattern I are engraved smoothly onto the 3D finger surface.

This preprocessing is not needed if any other calibration pattern (e.g. sine grating of certain orientation and frequency) is being projected.

2.3 Mapping 2D calibration pattern to 3D surface

The front portion S_{OF} of the outer finger surface S_O is projected from 3D ((x, y, z) coordinate space) to 2D ((u, v) coordinate space) by computing the ISOMAP embedding described in [24] (see Fig. 6). Recall that the vertices and triangles in S_{OF} are V_{OF} and T_{OF}, respectively. The ISOMAP embedding is computed by:

1) **Constructing adjacency graph**: An adjacency graph G is created, by connecting all vertex pairs $\{v_i, v_j\}$ in V_{OF} that share an edge of any triangle in T_{OF}. The edge weights in G are set to the euclidean distance $D(v_i, v_j)$ between the vertex locations. Note that for non-adjacent vertex pairs that do not share any edge, D is set to ∞.
2) **Computing shortest paths**: Dijkstra's shortest path algorithm [25] is used to compute the shortest path between all pairs of nodes in G. Geodesic distances between all pairs of vertices in V_{OF} are estimated by the shortest path distances of the nodes in G.
3) **Constructing 2D embedding**: Let the matrix D_G contain the shortest path distances computed in the previous step. Given D_G, classical multidimensional scaling (MDS) [26] is used to create the 2D embedding of vertices. MDS maintains the intrinsic geometry of the surface S_OF during the 3D to 2D projection.

ISOMAP embedding is used because it minimizes the distortion induced when projecting the front portion S_{OF}

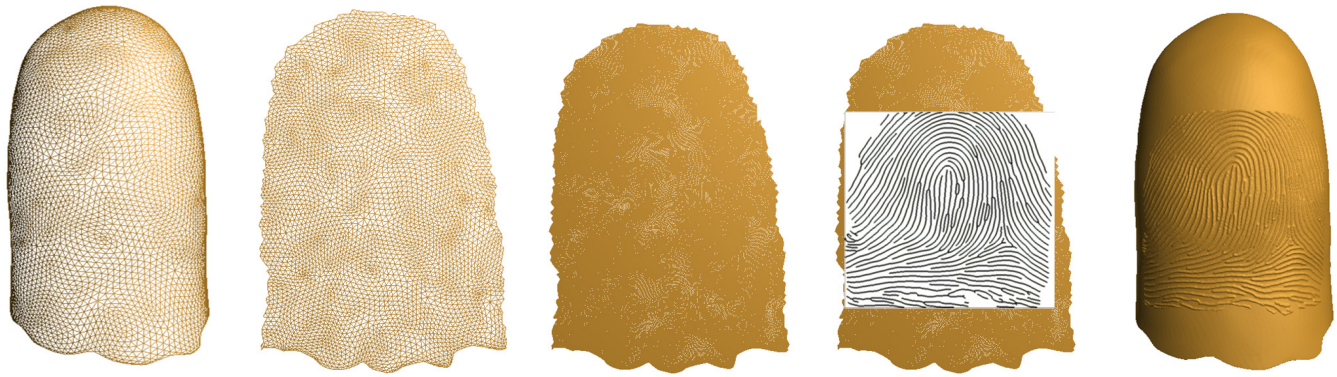

Fig. 6. Mapping and engraving a 2D calibration pattern onto the front portion of the outer 3D finger surface. (a) 3D frontal outer finger surface, (b) frontal surface in (a) is projected into 2D, (c) the 2D projected frontal surface is subdivided, (d) correspondences are determined between the 2D projected frontal finger surface and 2D calibration pattern, (e) 3D frontal outer finger surface in (a) is displaced along the surface normals to engrave the pattern.

of the 3D surface to 2D by preserving the geodesic distances between neighborhoood vertices on S_{OF} during the 3D to 2D projection[4].

Let the 2D projected frontal surface in the (u, v) coordinate space be denoted by S_{OFP} with the set of vertices V_{OFP} and the set of triangles T_{OFP}. Rotation and flip during the 3D to 2D projection of S_{OF} are corrected using corresponding control points between S_{OF} and S_{OFP}. Reference coordinates $[r_u, r_v]$ are extracted from the 2D calibration pattern I for translation correction during the 3D to 2D projection of S_{OF}:

- If the pattern I being projected is a synthetic fingerprint image, then reference coordinates $[r_u, r_v]$ are extracted from the fingerprint image using the method described in [27].
- If any other calibration pattern is being projected (e.g. sine gratings, horizontal/vertical bar patterns etc.) , then the location of the center pixel in the 2D calibration pattern I is used as the reference point i.e. $[r_u, r_v] = [w/2, h/2]$, where w and h are the width and height of the 2D pattern I.

The next step is to determine the one-to-one mapping between the pixel locations (u, v) on I and the vertices V_{OF} on S_{OFP}. For accurately determining the one-to-one correspondence, the density of S_{OF} as well as its 2D projection S_{OFP} is further increased using midpoint surface subdivision. Vertices are sampled on the midpoints of the edges in T_{OF}, and the sampled vertices on the adjacent edges are joined to create new triangles. The resolution of I being projected is factored into the computations while determining the correspondence between pixel locations on I and vertices V_{OF} on S_{OFP}. For example, if the calibration pattern being projected has a resolution of 500 ppi, the scale of projection is 19.685 pixels/mm. Therefore, the coordinates of I are scaled by this factor before determining the correspondence.

Ideally, the density of S_{OF} needs to be increased according to the dimensions of the I being projected. For example, if a calibration pattern of width w and height h is being projected, then exactly $w \times h$ vertices are required in the projection region for building the exact correspondence between the pixel locations on I and the vertices on S_{OF}. However, this is not recommended because it would result in a very large number of vertices and triangles on the surface and considerably increase the computational complexity of further processing on the surface. Therefore, the density of S_{OF} is only increased to a certain degree to retain the essential topology of the pattern being projected[5]. Let the set of vertices and triangles on the 2D projected frontal surface obtained after this step be denoted by V_{OFPS} and T_{OFPS}. The corresponding vertices and triangles on the outer 3D frontal surface be V_{OFS} and T_{OFS}, respectively. The one-to-one correspondence between the pixel locations on the calibration pattern I and the set of vertices V_{OFP} is then established.

2.4 Engraving 2D calibration pattern on 3D surface

In the penultimate step, surface normals are computed at each vertex in the set V_{OFPS}. The vertices are then displaced along their surface normals to engrave the fingerprint ridges and valleys on S_{OF} (see Fig. 6 (e)). Let the normal at a vertex v in the set V_{OFPS} be denoted by (n_x, n_y, n_z), where n_x, n_y and n_z represent the normal components along the x, y and z directions, respectively.

4. Discrete conformal mapping was used for projecting a 2D image to 3D finger surface in the earlier version of this paper [1]. It was, however, observed that discrete conformal mapping did not preserve the distances on the calibration pattern near the periphery of the 3D surface since it is an angle preserving mapping.

5. For the finger surface used in our experiments, the density is increased so that there are approximately 250,000 vertices and 500,000 triangles on the front portion of the 3D surface.

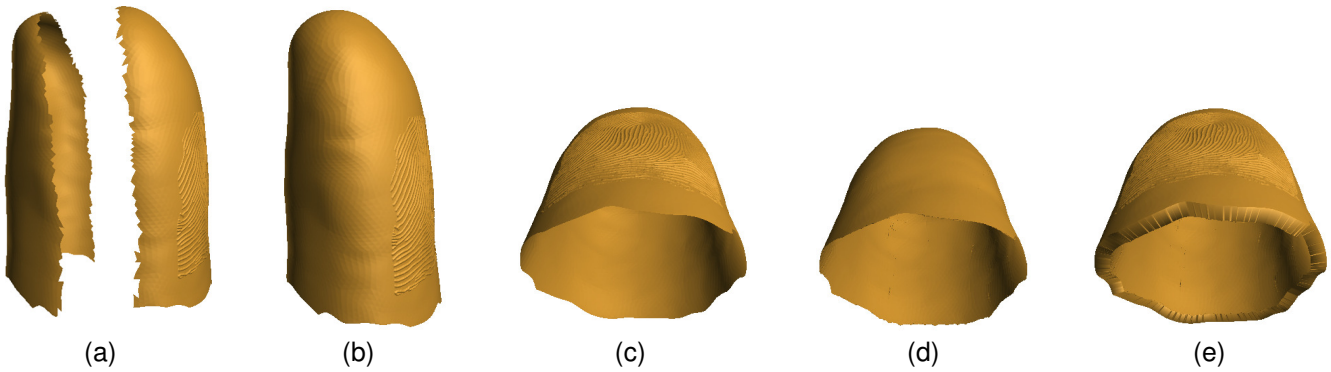

Fig. 7. Postprocessing 3D finger surface. (a) Separated front and rear portions of outer 3D surface, (b) front and rear portions shown in (a) are combined to create the outer 3D finger surface, (c) outer 3D finger surface (bottom view), (d) the retained original 3D finger surface (bottom view), (e) 3D electronic target created by stitching the outer and original surface in (c) and (d).

TABLE 2
Comparison of mechanical properties of the two different printing materials with the human finger skin.

Property	Human Skin [29] [30]	TangoBlackPlus FLX980 [31]	FLX 9840 -DM [32]
Shore A hardness	20-41	26-28	35-40
Tensile Strength (MPa)	5-30	0.8-1.5	1.3-1.8
Elongation at Break (%)	35-115	170-220	110-130

The displaced coordinates of the vertex (v'_x, v'_y, v'_z) along the normal are then computed using the principle of vertex displacement mapping [28] as follows:

$$\begin{bmatrix} v'_x \\ v'_y \\ v'_z \end{bmatrix} = \begin{bmatrix} v_x \\ v_y \\ v_z \end{bmatrix} + \begin{bmatrix} n_x \\ n_y \\ n_z \end{bmatrix} \times (1 - I'(u,v)) \times R_d \qquad (5)$$

Here, $I'(u,v)$ is the scale normalized texture value in the range $[0,1]$ of the mapped (u,v) texture from the 2D calibration pattern on the vertex v, and R_d is the maximum vertical ridge displacement which is set to 0.22 mm in our experiments[6].

2.5 Postprocessing 3D finger surface

The engraved S_{OF} and S_{OR} are then combined together to recreate the outer finger surface S'_O. The outer finger surface S'_O is then stitched together with the retained original finger surface S_O to create a continuous watertight 3D shell S_W ready for 3D printing. For doing this, the boundary of the two meshes S'_O and the S_O is first computed. Triangles are then synthetically generated to connect the two boundaries to create a continuous shell (see Fig. 7). This continuous watertight shell is basically the 3D target A in electronic form.

6. The average ridge height on an adult human fingerprint is about 0.06 mm; however we set R_d to 0.22 mm empirically due to limitation of the 3D printer resolution used for fabricating the targets.

2.6 3D printing

We use a state-of-the-art 3D printer (Stratasys Objet350 Connex) that has X and Y resolution of 600 dpi and Z resolution of 1600 dpi for fabricating the 3D targets with rubber-like materials. This printer is based on PolyJet printing technology which slices a 3D model into horizontal layers, and then prints the model layer by layer. The 3D targets are printed in high speed mode wherein they are sliced into 30 micrometer layers during the printing process. Note that the printer does not support printing the target with rubber-like materials in the high resolution mode which allows for even finer 16 micrometer layer slicing. However, we found that 30 micrometer slicing suffices with ridge displacement R_d of 0.22 mm. Note that in the high speed mode, the time taken to fabricate one 3D target using the printer is around 1.5 hrs.

Two different rubber-like materials, TangoBlackPlus FLX980 [31], and FLX 9840-DM [32] (a digital material synthesized in the printer using a rubber-like material and a rigid material) are used for printing the 3D targets. These materials are specifically selected because they are similar in hardness and elasticity to the human finger skin (see Table 2).

While printing the 3D targets, the printer uses a support material to prevent the models being fabricated from breaking. As a result, once the targets are printed they need to be cleaned to remove the support material. Although manual cleaning can remove most of the support material, often residue of the support material is left even after careful manual cleaning. Therefore, a high pressure water jet is used to clean the 3D printed models.

TABLE 3
Similarity scores between the captured snapshots of the 3D electronic targets in Meshlab and the fingerprint images used in their synthesis. Five fingerprints from the NIST SD4 were used. Verifinger 6.3 SDK was used for comparing fingerprints. The similarity threshold @FAR = 0.01% is 33.

Fingerprint	S0005	S0010	S0017	S0083	S0096
scores	171	378	212	116	106

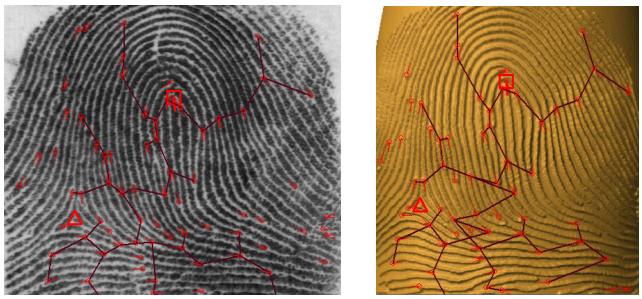

(a) (b)

Fig. 8. Feature comparison (minutiae, core and delta shown here) between (a) rolled fingerprint image (S0083) from the NIST SD4, and (b) snapshot of the electronic 3D target synthesized using the fingerprint in (a) using Verifinger 6.3 SDK. Similarity score of 116 is obtained between (a) and (b).

3 Fidelity of 3D Target Synthesis

Given that we synthesize 3D targets for evaluating fingerprint readers, it is important to assess if the synthesized targets are adequate in terms of their utility for this purpose. To determine the fidelity of 3D target synthesis, we evaluate the targets to determine if the

- features present in the 2D pattern, I, are preserved during projection to 3D to create the electronic (virtual) 3D target,
- features engraved on the electronic 3D finger surface are preserved after fabrication of the physical 3D target,
- features present in the 2D pattern, I, are preserved on the physical 3D target, and
- intra-class variability between the captured impressions of the 3D target using fingerprint readers is minimal.

Five different rolled fingerprint impressions from the NIST Special Database 4 (NIST SD4) [33] are projected onto a 3D finger surface to synthesize 3D targets. The targets are fabricated with each of the two fabrication materials using a state-of-the-art 3D printer (see Section 2.6). Three optical fingerprint readers (500/1000 ppi) are used for imaging the 3D targets[7]. A commercial fingerprint SDK [17] is used for conducting all matching experiments.

TABLE 4
Similarity scores between the captured snapshots of the 3D electronic targets and the captured impressions of the physical 3D targets fabricated with TangoBlackPlus FLX980 and FLX 9840-DM using the three optical readers. Five fingerprints from the NIST SD4 were used. Verifinger 6.3 SDK was used for comparing fingerprints. The similarity threshold @FAR = 0.01% is 33.

TangoBlackPlus FLX980

Fingerprint	OR 1 (500 ppi)	OR 2 (1000 ppi)	OR 3 (1000 ppi)
S0005	191	215	203
S0010	153	173	140
S0017	114	164	155
S0083	315	497	498
S0096	110	162	183

FLX 9840-DM

Fingerprint	OR 1 (500 ppi)	OR 2 (1000 ppi)	OR 3 (1000 ppi)
S0005	194	164	192
S0010	158	159	168
S0017	129	165	162
S0083	353	431	554
S0096	107	152	164

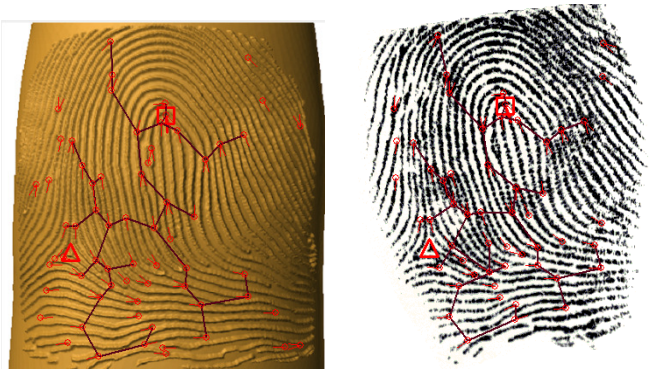

(a) (b)

Fig. 9. Feature comparison (minutiae, core and delta shown here) between (a) snapshot of the electronic 3D target synthesized using the fingerprint S0083 in NIST SD4, and (b) the captured impression by optical reader 2 (1000 ppi) of the physical 3D target fabricated with TangoBlackPlus FLX-980 using Verifinger 6.3 SDK. Similarity score of 497 is obtained between (a) and (b).

7. Capacitive fingerprint readers could not be used because state-of-the-art 3D printers currently do not allow printing objects using conductive materials. However, capacitive readers could be used provided that the targets are fabricated using conductive materials. We are currently exploring the possibility of using alternative fabrication methods.

TABLE 5
Similarity scores between the captured impressions of the 3D targets fabricated with TangoBlackPlus FLX980 and FLX 9840-DM using the three optical readers and the fingerprint impressions used in their synthesis. Five fingerprints from NIST SD4 were used. Verifinger 6.3 SDK was used for comparing the impressions. The similarity threshold @FAR = 0.01% is 33.

TangoBlackPlus FLX980

Fingerprint	OR 1 (500 ppi)	OR 2 (1000 ppi)	OR 3 (1000 ppi)
S0005	105	68	71
S0010	90	77	78
S0017	89	83	74
S0083	96	128	123
S0096	101	98	74

FLX 9840-DM

Fingerprint	OR 1 (500 ppi)	OR 2 (1000 ppi)	OR 3 (1000 ppi)
S0005	80	66	65
S0010	80	104	80
S0017	108	96	89
S0083	110	120	120
S0096	75	81	71

(a) (b)

Fig. 10. Feature comparison (minutiae, core and delta shown here) between (a) rolled fingerprint image (S0083) from the NIST SD4, and (b) the captured image using optical reader 2 (1000 ppi) of the 3D target synthesized using the fingerprint in (a) and fabricated with TangoBlackPlus FLX980 using Verifinger 6.3 SDK. Similarity score of 128 is obtained between (a) and (b).

3.1 Fidelity of 2D pattern features during projection to 3D surface

Each electronic 3D target is previewed in the 3D mesh processing software Meshlab [34], and its frontal snapshot is taken. The captured snapshot of the electronic 3D target is rescaled manually to the same scale as the original 2D fingerprint images used during the synthesis of the target. The rescaled snapshot images of the electronic 3D target is matched to the original 2D fingerprint image using the commercial fingerprint SDK.

Fig. 8 shows a sample fingerprint image from the NIST SD4 and the snapshot of an electronic 3D target. The features extracted and matched using the commercial fingerprint SDK are marked on the two images. Table 3 shows the obtained similarity scores for the experiment. All similarity scores are significantly above the verification score threshold of 33 (@FAR = 0.01%)for NIST SD4. It can, thus, be inferred that the features present in the 2D fingerprint image are preserved during the synthesis of the electronic 3D target.

TABLE 6
Range of similarity scores for pairwise comparisons between five impressions of the 3D targets fabricated with TangoBlackPlus FLX980 and FLX 9840-DM captured by the three optical readers. Five fingerprints from NIST SD4 were used in their synthesis. Verifinger 6.3 SDK was used for comparing the impressions. The similarity threshold @FAR = 0.01% is 33.

TangoBlackPlus FLX980

Fingerprint	OR 1 (500 ppi)	OR 2 (1000 ppi)	OR 3 (1000 ppi)
S0005	581-1370	902-1643	846-1394
S0010	696-1656	534-1463	819-1194
S0017	900-1171	945-1478	515-1284
S0083	831-1935	1466-1836	1364-1746
S0096	707-1170	812-1392	984-1287

FLX 9840-DM

Fingerprint	OR 1 (500 ppi)	OR 2 (1000 ppi)	OR 3 (1000 ppi)
S0005	417-1514	990-1439	890-1494
S0010	659-1196	906-1292	1043-1355
S0017	1016-1937	1088-1482	1326-1571
S0083	810-1520	1193-1547	1356-1757
S0096	459-1062	1352-1496	1127-1511

3.2 Fidelity of the engraved features on the 3D surface after 3D printing

The snapshot of an electronic 3D target is matched to captured impression of the physical 3D target using the three optical readers for each of the ten 3D targets. Fig. 9 shows feature comparison obtained using the commercial fingerprint SDK between the snapshot of one electronic target and its captured impression using one optical reader. Table 4 shows the obtained scores for this experiment. Notice that the similarity scores are significantly above the verification threshold score of 33 (@FAR = 0.01%) for all targets. This demonstrates the fidelity of features engraved on the 3D surface after 3D printing.

3.3 End-to-end fidelity of 2D pattern features after 3D printing

Table 5 shows the similarity scores obtained on matching the captured impressions of the 3D target to the original fingerprint for each of the five 3D targets printed with the two materials and imaged using the three readers. Fig. 10 shows feature comparison between the fingerprint

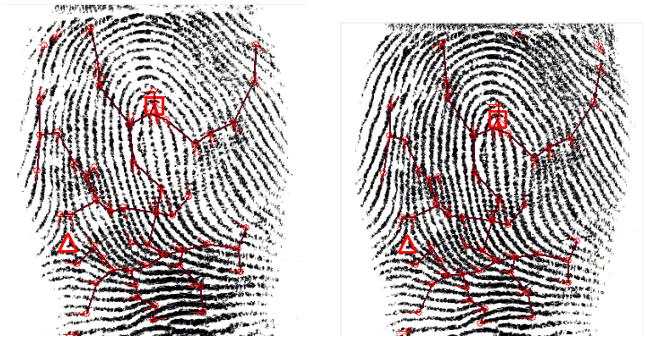

(a) (b)

Fig. 11. Feature comparison (minutiae, core and delta shown here) between two captured impressions (a) and (b) using optical reader 2 (1000 ppi) of a 3D target fabricated with TangoBlackPlus FLX980 using Verifinger 6.3 SDK. The 3D target was synthesized using a rolled fingerprint image (S0083) in NIST SD4. Similarity score of 1592 is obtained between (a) and (b).

image and captured impressions of the synthesized 3D target using the commercial fingerprint SDK. The key observations and inferences based on this experiment are:

- The captured images of the 3D targets using the three optical readers can be successfully matched to the original fingerprint images used for synthesizing the targets with high confidence. This is because all similarity scores (see Table 5) are significantly above the verification threshold score of 33 (@FAR = 0.01%) computed for the NIST SD4.
- Because the captured images of the 3D targets can be successfully matched to the original fingerprint images (@FAR = 0.01%), it can be inferred that the salient features present in the 2D pattern are preserved during the fabrication of the physical 3D target.

3.4 Intra-class variability between 3D target impressions

Five different impressions of each of the ten 3D targets are captured using each of the three optical readers. Pairwise comparisons between the five impressions obtained from a reader are performed using the commercial fingerprint SDK. Fig. 11 shows the extracted and matched features by the fingerprint SDK between two impressions of a 3D target captured using the three readers. Table 6 shows the range of similarity scores obtained for this experiment. It is observed that the similarity scores obtained are significantly higher than the verification threshold, thereby, indicating that the intra-class variability between multiple different captured impressions of the 3D target is minimal. In other words, different impressions of the 3D target are fairly consistent.

TABLE 7
Mean (μ) and std. deviation (σ) of computed center-to-center spacing in the acquired images of the three test targets using the three optical readers. (original grating spacing = 10 pixels)

Test pattern	OR 1 (500 ppi)	OR 2 (1000 ppi)	OR 3 (1000 ppi)
Horizontal	μ = 9.04, σ = 0.06	μ = 9.18, σ = 0.07	μ = 9.05, σ = 0.05
Vertical	μ = 9.51, σ = 0.23	μ = 9.57, σ = 0.07	μ = 9.46, σ = 0.09
Circular	μ = 9.80, σ = 0.31	μ = 9.62, σ = 0.07	μ = 9.59, σ = 0.08

4 Evaluating Fingerprint Readers Using 3D Targets

For evaluating the fingerprint readers, three different 3D targets are created by projecting synthetically generated 2D test patterns: (i) horizontal, (ii) vertical, and (iii) circular gratings with a fixed center-to-center spacing of 10 pixels. Ten different impressions of each of the three targets are captured using the three optical readers. Center-to-center spacing is then measured in each of the captured impressions using the method in [35]. Fingerprint readers are subsequently evaluated based on how well the grating spacings on the three targets is recovered by the readers. Figs. 12, 13 and 14 show the three test patterns, the electronic targets generated using the three patterns, and some sample images of the three targets captured using the three optical fingerprint readers.

The average and standard deviation of the observed center-to-center spacings in the captured impressions of the three targets is reported in Table 7. Note that to compensate for the distortion induced during 2D to 3D projection of the 2D pattern, the ratio of the Euclidean distance on the pattern to Geodesic distance (0.94) on the 3D finger surface is factored into spacing computations. Following are some observations based on this experiment:

- The observed spacing, on average, is greater than 9 pixels in the captured images of all three targets using the three readers. The three readers, therefore, image the three targets with accuracies greater than 90%.
- The spacing in images of the horizontal target is, on average, less than those of the vertical target for all three optical readers. In other words, the readers better capture vertical spacings than horizontal spacings.
- The 500 ppi optical reader (OR 1) has a greater variation in the observed spacings in the captured images compared to the 1000 ppi readers (OR 2 and OR 3). This is because OR 1 images a smaller portion of the targets, and depending on how the user places the finger on the platen, the captured portion of the target differs between different impressions.

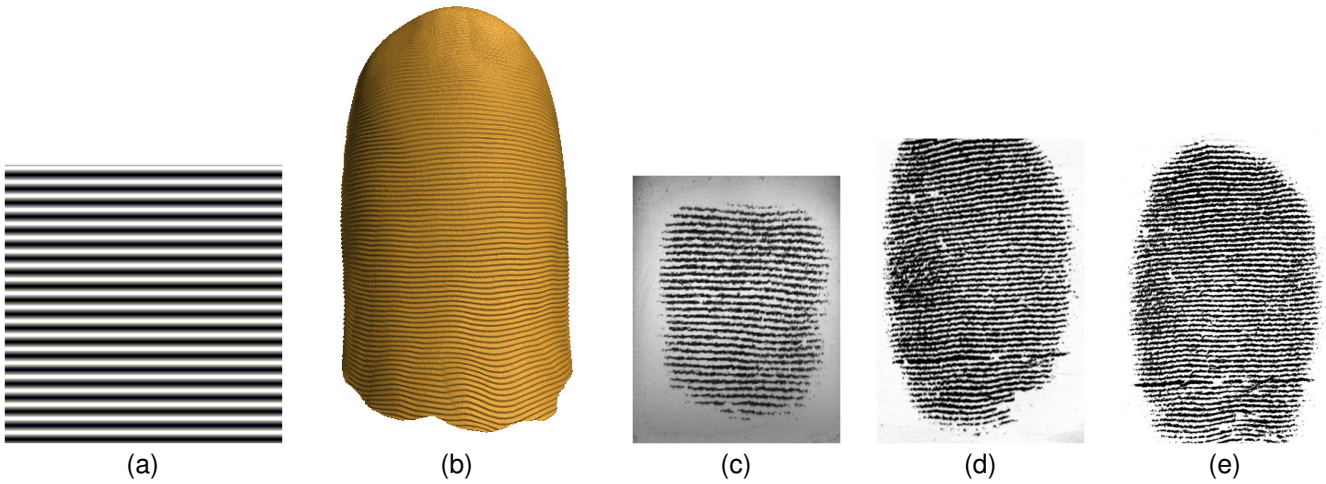

Fig. 12. Evaluating fingerprint readers using a 3D target synthesized from a horizontal sine grating. (a) Horizontal sine grating (10 pixels); (b) electronic 3D target synthesized using (a); (c),(d) and (e) are sample impressions of the fabricated target captured using optical readers 1, 2 and 3, respectively.

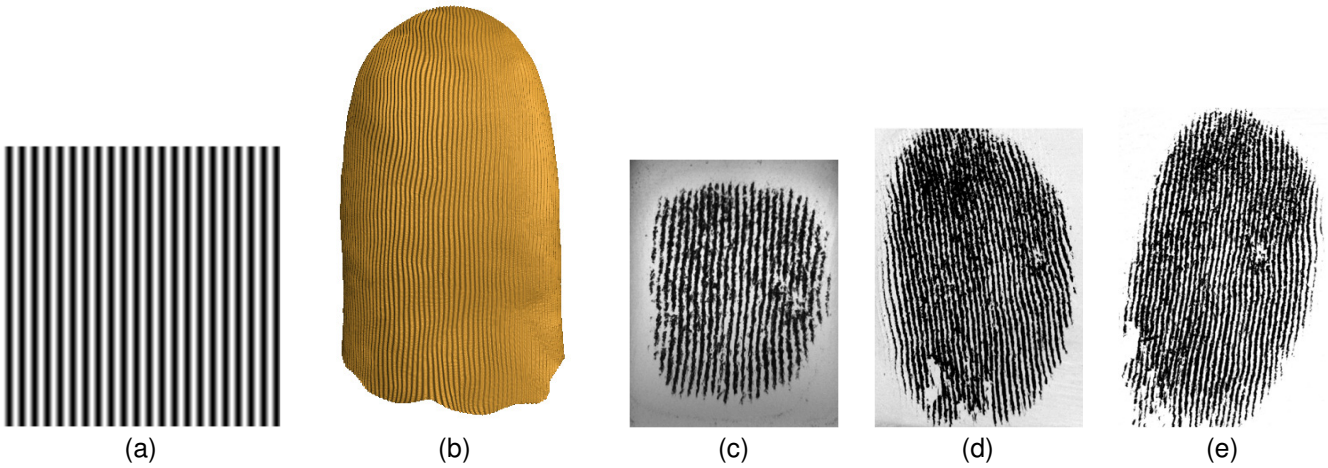

Fig. 13. Evaluating fingerprint readers using a 3D target synthesized from a vertical sine grating. (a) Vertical sine grating (10 pixels); (b) electronic 3D target synthesized using (a); (c),(d) and (e) are sample impressions of the fabricated target captured using optical readers 1, 2 and 3, respectively.

5 Conclusions and Ongoing Work

Calibration of fingerprint readers is typically done using 2D/3D targets designed for calibrating imaging devices. These targets are suitable for calibrating the imaging pathway of fingerprint readers. However, they cannot be used for repeatable operational evaluation of fingerprint readers. In this research, we have designed and fabricated wearable 3D targets which can be worn on a finger, placed on the reader platen, and imaged analogous to operational setting for evaluating fingerprint readers. The 3D targets are created by projecting 2D calibration patterns of known characteristics (e.g. sine gratings of known spacings) onto a generic 3D finger surface, and are fabricated using a state-of-the-art 3D printer with materials similar in hardness and elasticity to the human finger skin. Our experimental results show that (i) our 3D targets can be imaged by three different commercial optical fingerprint readers, (ii) features present in the 2D calibration patterns are generally preserved during the projection of the 2D pattern to synthesize electronic 3D targets, (iii) features engraved on the electronic 3D targets are generally preserved after fabricating physical 3D targets, and (iv) the intra-class variability between multiple images of the same 3D target captured using three different optical fingerprint readers is small. Experiments are also conducted to evaluate the three optical readers using the fabricated 3D targets.

We are currently investigating alternative methods to fabricate the 3D targets with higher precision. We are

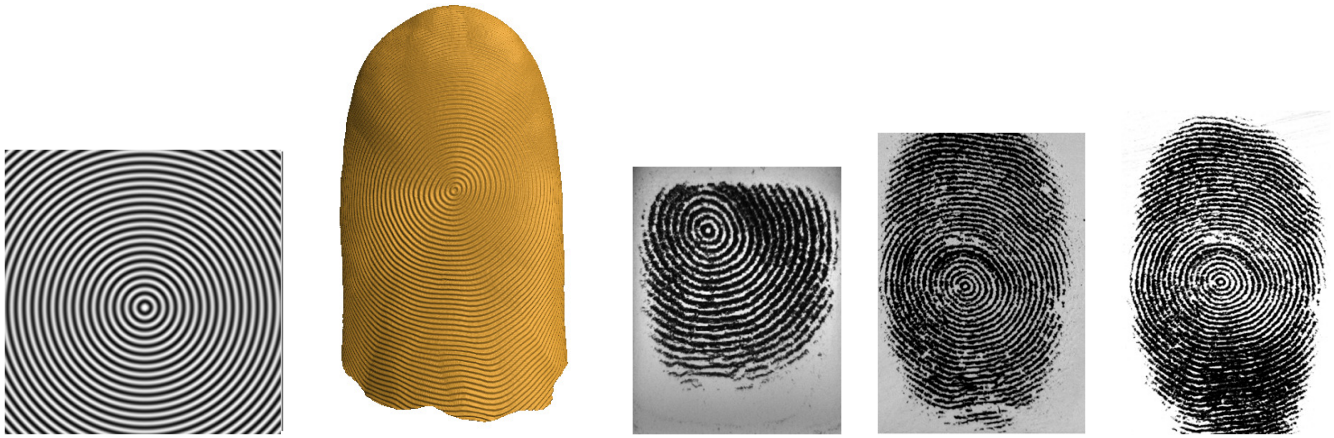

Fig. 14. Evaluating fingerprint readers using a 3D target synthesized from a circular sine grating. (a) Circular sine grating (10 pixels); (b) electronic 3D target synthesized using (a); (c),(d) and (e) are sample impressions of the fabricated target captured using optical readers 1, 2 and 3, respectively.

also investigating the possibility of using materials with similar optical properties and conductivity to the human finger skin to fabricate 3D targets for evaluating both optical and capacitive fingerprint readers. In future, we plan to simulate the effects of dry and worn fingers using 3D targets with different depths of engravings to further study the imaging capabilities of different readers.

ACKNOWLEDGMENTS

This research was supported by grant no. RC100915 from the NIST Measurement Science program. The authors would like to acknowledge Brian Wright, Michigan State University for his assistance in printing the 3D targets.

REFERENCES

[1] S. S. Arora, K. Cao, A. K. Jain, and N. G. Paulter, "3D Fingerprint Phantoms," in *22nd International Conference on Pattern Recognition (ICPR)*, 2014, pp. 684–689.

[2] V. V. Tuchin, A. N. Bashkatov, E. A. Genina, V. I. Kochubey, V. V. Lychagov, S. A. Portnov, N. A. Trunina, D. R. Miller, S. Cho, H. Oh, B. Shim, M. Kim, J. Oh, H. Eum, Y. Ku, D. Kim, and Y. Yang, "Finger tissue model and blood perfused skin tissue phantom," pp. 78 980Z–78 980Z–11, 2011. [Online]. Available: http://dx.doi.org/10.1117/12.881604

[3] D. A. Boas, C. Pitris, and N. Ramanujam, *Handbook of Biomedical Optics*. Taylor & Francis, 2011.

[4] N. B. Nill, "Test procedures for verifying image quality requirements for personal identity verification (PIV) single finger capture devices," MITRE, Tech. Rep. MTR 060170, 2006.

[5] "FBI Biospecs IAFIS FAQs," https://www.fbibiospecs.org/iafis_faq.html.

[6] N. B. Nill, "Test procedures for verifying IAFIS image quality requirements for fingerprint scanners and printers v 1.4," MITRE, Tech. Rep. MTR 05B0016R7, 2013.

[7] "FBI IAFIS certified product listing," http://www.fbi.gov/about-us/cjis/fingerprints_biometrics/iafis/iafis_cert.

[8] "UID Biometric Device Certification," http://www.uidai.gov.in/biometric-device-certification.html.

[9] J. Daugman, "600 million citizens of india are now enrolled with biometric id." [Online]. Available: http://spie.org/x108321.xml

[10] "Biometric Design Standards for UID Applications v 1.0," *UIDAI Committee on Biometrics*, Dec 2009. [Online]. Available: http://www.uidai.gov.in/UID_PDF/Committees/Biometrics_Standards_Committee_report.pdf

[11] "Guidance to applicant for biometric devices for UID Application (BDCS-03-02)," *STQC IT Services*, Dec 2010. [Online]. Available: http://www.uidai.gov.in/images/commdoc/guidance_to_applicant.pdf

[12] R. Cappelli, "SFinGe: an approach to synthetic fingerprint generation," in *International Workshop on Biometric Technologies (BT2004)*, 2004, pp. 147–154.

[13] IBG, "Synthetic biometric image generator," *Department of Homeland Security Small Business Innovation Research Final Report*, 2012.

[14] Q. Zhao, A. Jain, N. Paulter, and M. Taylor, "Fingerprint image synthesis based on statistical feature models," in *IEEE Fifth International Conference on Biometrics: Theory, Applications and Systems (BTAS)*, 2012, pp. 23–30.

[15] "Thor Labs Calibration Targets," http://www.thorlabs.com/newgrouppage9.cfm?objectgroup_id=7502.

[16] "Artec Eva 3D scanner," http://www.artec3d.com/hardware/artec-eva/.

[17] "Neurotechnology Verifinger SDK 6.3," http://www.neurotechnology.com/verifinger.html.

[18] I. Jolliffe, *Principal Component Analysis*. Wiley Online Library, 2005.

[19] G. Peyré and L. D. Cohen, "Geodesic remeshing using front propagation," *International Journal of Computer Vision*, vol. 69, no. 1, pp. 145–156, 2006.

[20] R. Kimmel and J. A. Sethian, "Computing geodesic paths on manifolds," *Proceedings of the National Academy of Sciences*, vol. 95, no. 15, pp. 8431–8435, 1998.

[21] P. Alliez, D. Cohen-Steiner, O. Devillers, B. Lévy, and M. Desbrun, "Anisotropic polygonal remeshing," in *ACM Transactions on Graphics (TOG)*, vol. 22, no. 3. ACM, 2003, pp. 485–493.

[22] N. Amenta, M. Bern, and D. Eppstein, "The crust and the β-

skeleton: Combinatorial curve reconstruction," *Graphical models and image processing*, vol. 60, no. 2, pp. 125–135, 1998.

[23] C. Loop, "Smooth subdivision surfaces based on triangles," Master's thesis, University of Utah, 1987.

[24] J. B. Tenenbaum, V. De Silva, and J. C. Langford, "A global geometric framework for nonlinear dimensionality reduction," *Science*, vol. 290, no. 5500, pp. 2319–2323, 2000.

[25] E. Dijkstra, "A note on two problems in connexion with graphs," *Numerische Mathematik*, vol. 1, no. 1, pp. 269–271, 1959. [Online]. Available: http://dx.doi.org/10.1007/BF01386390

[26] J. B. Kruskal and M. Wish, *Multidimensional Scaling*. Sage, 1978.

[27] S. Yoon, K. Cao, E. Liu, and A. K. Jain, "LFIQ: Latent fingerprint image quality," in *IEEE Sixth International Conference on Biometrics: Theory, Applications and Systems (BTAS)*, 2013, pp. 1–8.

[28] "Vertex Displacement Mapping using GLSL," http://www.ozone3d.net/tutorials/vertex_displacement_mapping_p02.php.

[29] C. Edwards and R. Marks, "Evaluation of biomechanical properties of human skin," *Clinics in Dermatology*, vol. 13, no. 4, pp. 375–380, 1995.

[30] V. Falanga and B. Bucalo, "Use of a durometer to assess skin hardness," *Journal of the American Academy of Dermatology*, vol. 29, no. 1, pp. 47–51, 1993.

[31] "Stratasys Polyjet Material Data Sheet," http://www.stratasys.com/~/media/Main/Secure/Material%20Specs%20MS/PolyJet-Material-Specs/PolyJet_Materials_Data_Sheet.pdf.

[32] "Stratasys Digital Materials (DMs) Data Sheet," http://www.stratasys.com/~/media/Main/Secure/Material%20Specs%20MS/PolyJet-Material-Specs/Digital_Materials_Datasheet.pdf.

[33] "NIST Special Database 4," http://www.nist.gov/srd/nistsd4.cfm.

[34] "Meshlab," http://sourceforge.net/projects/meshlab/.

[35] L. Hong, Y. Wan, and A. K. Jain, "Fingerprint image enhancement: algorithm and performance evaluation," *IEEE Transactions on Pattern Analysis and Machine Intelligence*, vol. 20, no. 8, pp. 777–789, 1998.

Sunpreet S. Arora received the Bachelor of Technology (Hons.) degree in Computer Science from the Indraprastha Institute of Information Technology, Delhi (IIIT-D) in 2012. He is currently a doctoral student in the Department of Computer Science and Engineering at Michigan State University. His research interests include biometrics, pattern recognition and image processing. He was awarded the prestigious National Talent Search (NTS) scholarship by the National Council of Educational Research and Training (NCERT), India in 2006. He received the best poster award at the IEEE Fifth International Conference on Biometrics: Theory, Applications and Systems (BTAS), 2012. He is a student member of the IEEE.

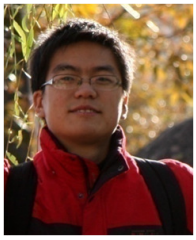

Kai Cao received the Ph.D. degree from Key Laboratory of Complex Systems and Intelligence Science, Institute of Automation, Chinese Academy of Sciences, Beijing, China, in 2010. He is currently a Post Doctoral Fellow in the Department of Computer Science & Engineering, Michigan State University, East Lansing. He is also with Xidian University as an associate professor. His research interests include biometric recognition, image processing and machine learning.

Anil K. Jain is a University distinguished professor in the Department of Computer Science and Engineering at Michigan State University. His research interests include pattern recognition and biometric authentication. He served as the editor-in-chief of the IEEE TRANSACTIONS ON PATTERN ANALYSIS AND MACHINE INTELLIGENCE (1991-1994). The holder of eight patents, he is the author of a number of books, including Handbook of Fingerprint Recognition (2009), Handbook of Biometrics (2011), Handbook of Multibiometrics (2006), Handbook of Face Recognition (2005), BIOMETRICS: Personal Identification in Networked Society (1999), and Algorithms for Clustering Data (1988). He served as a member of the Defense Science Board and The National Academies committees on Whither Biometrics and Improvised Explosive Devices. Dr. Jain received the 1996 IEEE TRANSACTIONS ON NEURAL NETWORKS Outstanding Paper Award and the Pattern Recognition Society best paper awards in 1987, 1991, and 2005. He is a fellow of the AAAS, ACM, IAPR, and SPIE. He has received Fulbright, Guggenheim, Alexander von Humboldt, IEEE Computer Society Technical Achievement, IEEE Wallace McDowell, ICDM Research Contributions, and IAPR KingSun Fu awards.

Nicholas G. Paulter Jr. is the Group Leader for the Security Technologies Group and is a former Program Manager for the Detection, Enforcement, and Inspection program of the Law Enforcement Standards Office (OLES) at NIST in Gaithersburg, MD. He develops and oversees metrology programs related to concealed-weapon detection, through-wall surveillance, traffic control devices, imaging for security and emergency response applications, biometrics for identification, and weapon output characterization. In this role, he has initiated two NIST programs in sub-millimeter-wave concealed weapon imaging, facilitated the development of visible-light hyper-spectral image projection, initiated a NIST-centric imaging metrology program for security and emergency applications, started two through-wall surveillance/sensing metrology activities, and started a program for characterization of the high-voltage output of electroshock weapons. He was awarded a NIST Bronze Medal in 2003 for his work in developing minimum performance requirements for metal detectors. Prior to being a Program Manager in OLES, from 1990 to 2005, Mr. Paulter was the Leader for the High-Speed Pulse Metrology Project at NIST. In that capacity, he developed several high-speed electrical pulse generation and sampling systems, electro-optic based measurement systems, and short optical pulse laser systems for use in pulse metrology. Moreover, during his tenure as the Project Leader, the metrology services provided by his project became the best in the world.

From 1980 to 1989, Mr. Paulter was with Los Alamos National Laboratory, Los Alamos, NM, and was involved in the study of fast electrical and optical phenomena. Mr. Paulter has authored or co-authored over 100 peer-reviewed technical articles and provided numerous presentations at a variety of technical conferences. His is a 2008-2009 Commerce Science and Technology Fellow and a 2010 IEEE Fellow; and received a B.S. in biological sciences from the University of California, Santa Barbara in 1980; an M.S. in chemistry from the University of New Mexico in 1988; and an M.S. in electronics engineering from the University of Colorado Boulder in 1990.